Preprint
UCRL-JC-140919

Application of Constrained-Layer Damping to a Precision Kinematic Coupling

S. A. Jensen, L. C. Hale

This article was submitted to
International Modal Analysis Conference, Kissimee, FL., February 5-8, 2001

U.S. Department of Energy
Lawrence Livermore National Laboratory

October 10, 2000

This work was performed under the auspices of the United States Department of Energy by the University of California, Lawrence Livermore National Laboratory under contract No. W-7405-Eng-48.

Application of Constrained-Layer Damping to a Precision Kinematic Coupling

Steven A. Jensen and **Layton C. Hale**

Lawrence Livermore National Laboratory
7000 East Avenue
Livermore, CA. 94550

ABSTRACT

This paper addresses the need to support a very precise optical instrument while causing essentially no influence to its natural shape. Such influences could come from a number of sources, such as manufacturing tolerances, temperature changes, over-constrained structural members, or ground motion. Kinematic couplings have long been used for purposes of repeatable location and minimal influence to the supported object, however these couplings typically offer very little damping. This paper presents a kinematic coupling that utilizes constrained-layer damping techniques to damp out the first three modes of vibration of a precision optical instrument. Finite element analysis was used to aid in the design and tuning of the dampers for the kinematic coupling. Experimental tests were conducted and confirmed the effectiveness of the dampers. The quality factor *(Q)*, which measure the amplification at resonance, dropped from 33.3 to 5.9 on the first mode, from 156.3 to 7.1 on the second mode, and from 147.1 to 18.5 on the third mode. These dampers help to ensure that the stringent vibration requirements necessary to produce high quality optical images are met.

NOMENCLATURE

x, y, z	translational degrees of freedom / coordinates
α	relative visco-elastic stiffness (non-dimensional)
k	stiffness
η	loss factor
Q	quality factor
ζ	damping factor
A	surface area
E	Young's modulus
G	shear modulus
ν	Poisson's ratio
r	ratio between constraining-layer stiffness and structural stiffness
t	thickness
i	$\sqrt{-1}$

BACKGROUND

Extreme ultraviolet lithography (EUVL) is one of the leading candidates for patterning semiconductor devices during the next decade. The projection optics system for EUVL requires precise and repeatable alignment of the reflective optics within the structural housing. It is critical that the housing be isolated from variable loads that could change the optical alignment. Such loads could arise from being mounted to other structures in an over-constrained manner. This leads to uncertainty in predicted forces and deformations and ultimately results in imprecision. In addition to concern over quasi-static loads on the housing, the dynamic response of the projection optics system is also very demanding. The mount must be stiff to achieve sufficiently high resonant frequencies (> 100 Hz) and, if possible, provide moderate damping (> 5% critical) to reduce amplification at resonance. Together, these traits reduce the vibration amplitude of the optics caused by random ground motion transmitted through the vibration isolators.

Kinematic couplings (e.g., a three-vee coupling) are commonly used for the purposes of repeatable location and minimal influence to the supported object; however, typical kinematic couplings provide very little damping. This paper presents a unique kinematic coupling that utilizes constrained-layer damping techniques to damp out the first three modes of vibration on the EUVL projection optics system.

FLEXURE MECHANISM DESIGN

Figure 1a schematically shows the damped flexure mechanism used to support the EUVL projection optics system. This flexure mechanism will be referred to as a "bipod flexure", and a total of three are required for rigid support purposes (see *Figure 1b*). The ball-cone interface is used to provide connect-disconnect repeatability and allows three rotational degrees of freedom about the ball center. A pair of blade flexures (one in each leg of the bipod flexure) provides an additional hinge axis that in combination with the ball-cone joint releases one translational constraint. The remaining two translational

constraints are equivalent to those provided by a ball-vee interface typical of a three-vee kinematic coupling. The advantages of the ball-cone interface over the ball-vee interface are lower contact stress, higher stiffness and lower friction due to its small radius compared to the separation between the ball and hinge axis.

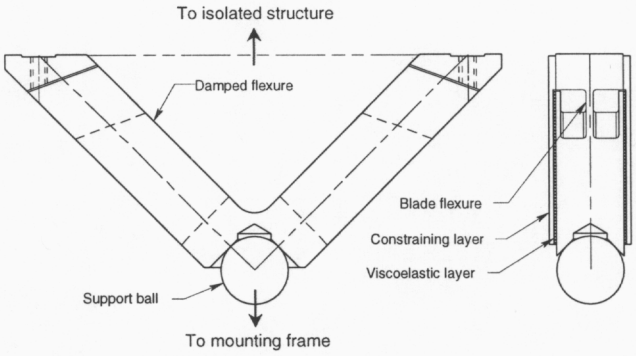

Figure 1a: Schematic of bipod flexure.

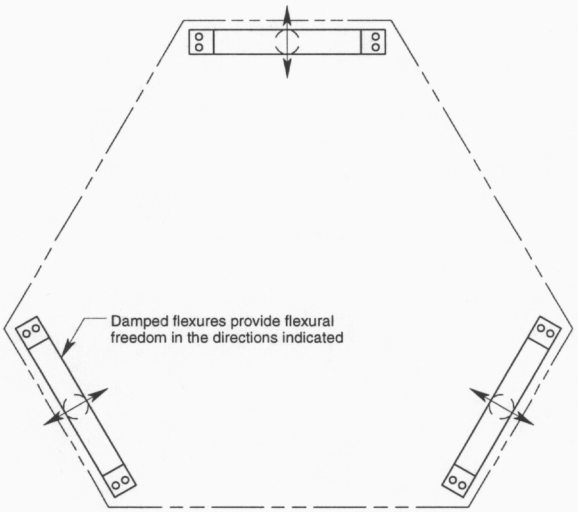

Figure 1b: Top view of support configuration, using 3 bipod flexures.

The constrained-layer damping treatment was applied in parallel (structurally) with the blade flexure with the intent to dampen vibration traveling axially along the length of each bipod leg (see *Figure 2*). This was done because the majority of vibration energy travels along the stiffest path and the support flexures were designed to be stiffest in the axial direction.

For convenience in describing how the dampers were constructed, each bipod leg will be divided into two sections, namely Section A and Section B (see *Figure 2a*). Section A refers to that portion of the bipod leg between the mounting holes and the base of the main flexure blade. Section B refers to that portion of the bipod leg from the base of the main flexure blade down towards the ball.

The bipod flexure was designed to have a main load-carrying flexure blade and two side webs on each leg. The webs and main flexure blade are cut from bulk material using an electro-discharge machining (EDM) process so that the entire part is monolithic. The webs, by themselves, provide no structural stiffness since they do not connect to Section A. These webs protect the main flexure blade from over-flexing and provide an area on which the visco-elastic material can be applied. The constraining layers are thin plates, having the same thickness as the webs, and are fastened to Section A with epoxy and screws. The visco-elastic material, which has adhesive on both sides, then binds the constraining layers to the side webs.

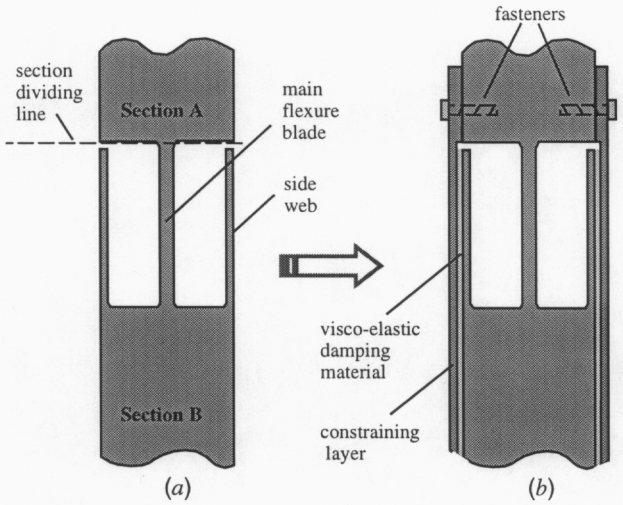

Figure 2: Side view of bipod leg, *a*) without damping treatment and *b*) with damping treatment.

CONSTRAINED-LAYER DAMPING

The damping mechanism in constrained-layer damping relies on the selected visco-elastic material (VEM) and its corresponding loss factor. The loss factor ($\eta = 1/Q$) is a direct measure of damping and is approximately twice the damping ratio (ζ) in a second order system. There are many different types of VEM, each possessing different loss factors over varying ranges of frequency and temperature. The VEM is applied between the structure to be damped and a stiffener, or constraining-layer, so that relative motion between them shears the VEM and dissipates energy. The application of VEM to a structure is most effective when it is impedance matched to the system, which requires analysis and/or measurement to achieve optimal performance. Without an analytical approach to damper design, it is easy to miss the optimal damping by a factor of three or more.

When modeling the dynamics of a structure, it is convenient to represent the individual modes using mass-spring-damper systems. When the damping element is visco-elastic rather than strictly viscous, the constitutive model uses the complex stiffness, where the loss factor is equal to the imaginary part divided by the real part. The

assumption is that the damping force is proportional to the displacement rather than the rate, which implies that it is independent of frequency. This is not entirely true because both the loss factor and shear modulus of a real VEM are frequency dependent, but the changes are small over the damping dominated region of a particular mode.

The simple spring system depicted in *Figure 3* below represents the structural connection between sections A and B shown in *Figure 2b*.

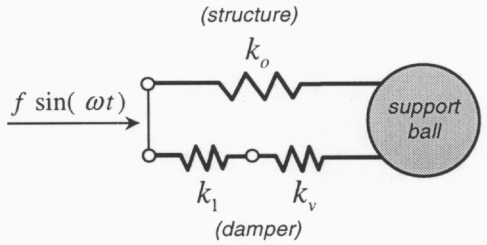

Figure 3: Spring model of bipod flexure leg with constrained-layer damping treatment.

The main flexure blade, having stiffness k_o, and the constrained-layer dampers act in parallel since they experience the same displacement. The constrained-layer damper is conveniently represented with two spring elements in series since both elements experience the same load; the VEM acting in shear having a stiffness of k_v, and the extension or compression of the constraining layers and webs lumped together having a stiffness of k_1. Since the constraining-layers and webs are much stiffer than the visco-elastic layer, shear deformation occurs across the visco-elastic layer when cyclical loads are transmitted. This shearing effect dissipates energy and reduces the vibration amplitude.

The equivalent stiffness of the spring model shown in *Figure 3* is described mathematically as follows:

$$k_{eq} = k_o + \frac{k_1 \cdot k_v}{k_1 + k_v} \tag{1}$$

Using the concept of complex stiffness, the following relationship is defined:

$$\frac{k_v}{k_1} \equiv \alpha(1 + i\eta) \tag{2}$$

where α is a non-dimensional parameter that indicates the relative visco-elastic stiffness and η is the loss factor of the VEM.

By way of substitution, the equivalent stiffness described in equation (1) can be rewritten as:

$$k_{eq} = k_o + k_1 \left[\frac{\alpha(1+i\eta)}{1+\alpha(1+i\eta)} \right] \tag{3}$$

Equation (3) indicates the nature of the optimization that must take place in determining the appropriate value of the visco-elastic stiffness (k_v) given a limiting constraining-layer stiffness (k_1). It shows that the damping in the system approaches zero as α approaches either zero or infinity. With these limits, the equivalent stiffness would be written as follows:

$$k_{eq}\Big|_{\alpha \to 0} \to k_o, \quad \text{and} \quad k_{eq}\Big|_{\alpha \to \infty} \to k_o + k_1 \tag{4}$$

The first step in the development of the optimal damper design requires separating k_{eq} into real and imaginary parts as shown in equation (5) below:

$$\frac{k_{eq}}{k_o} = \left[1 + r \frac{\alpha(1 + i\eta)}{1 + \alpha(1 + i\eta)} \right] \cdot \left(\frac{1 + \alpha(1 + i\eta)}{1 + \alpha(1 + i\eta)} \right) \tag{5}$$

$$= \frac{1 + (2 + r)\alpha + (1 + r)\alpha^2(1 + \eta^2) + i\eta r\alpha}{1 + 2\alpha + \alpha^2(1 + \eta^2)}$$

where r is the ratio of the constraining-layer stiffness to the structural stiffness, ($r = k_1 / k_o$). The relationship for each part is shown plotted in *Figure 4* as a function of α for η=1 and r = 1.

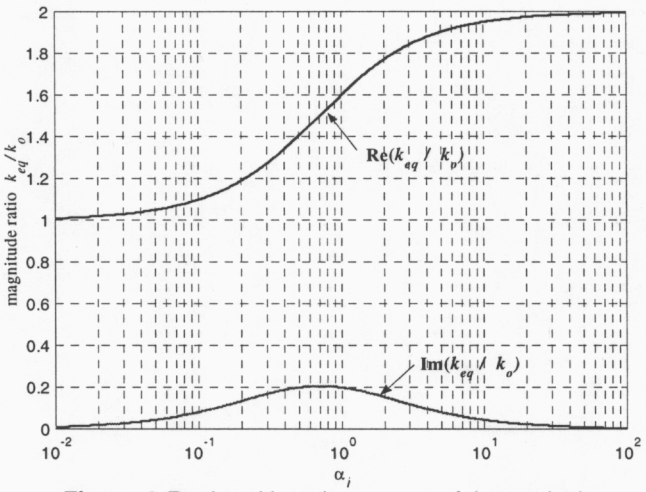

Figure 4: Real and imaginary parts of the equivalent stiffness $k_{eq}(\eta,r,\alpha)$ vs. α for r=1 and η=1.

As expected, the real part of the stiffness increases with α from k_o to $k_o + k_1$ and the imaginary part, which represents the damping, has a maximum that coincides with the real part being midway between k_o and $k_o + k_1$. It can be seen from equation (5) that the imaginary stiffness increases with r and η, however the practical limits for both are approximately 1. A stiffness ratio (r) greater than one is usually difficult to obtain due to other constraints and the mode shape is likely to change in a way to lessen the benefit of a larger ratio. The usual design strategy is to make r as large as practical and to select a high-loss visco-elastic material with the appropriate shear modulus and thickness to maximize some indicator of the damping.

The maximum imaginary stiffness occurs when the derivative with respect to α is zero, giving rise to equation (6) for α_{opt}. The optimum equivalent stiffness, shown in eqution (7), results from substituting α_{opt} into equation (5).

$$\mathrm{Im}\left(\frac{\partial k_{eq}}{\partial \alpha}\right) = 0 \quad \Rightarrow \quad \alpha_{opt} = (1+\eta^2)^{-\frac{1}{2}} \tag{6}$$

$$\left.\frac{k_{eq}}{k_o}\right|_{opt} = \frac{2+r}{2} + \frac{i\eta r}{2+2\sqrt{1+\eta^2}} \tag{7}$$

The difficulty in applying this model to a real system lies first in determining r for the particular application and then determining the visco-elastic stiffness to achieve α_{opt}. This is not too difficult for a damped beam structure by assuming a deflection shape and integrating the strain energies that correspond to k_o, k_1 and k_v. More complicated structures generally require a finite element approach such as a modal strain energy method. However, the equations developed from the spring model are useful to augment and check the modal strain energy approach.

MODAL TESTING OF BIPOD SUPPORT FLEXURES WITHOUT DAMPING TREATMENT ADDED

The structure that houses the projection optics is referred to as the projection optics box (POB). The POB is supported by the bipod flexures, which kinematically interface to a structure, referred to as the engineering test stand (ETS), through the ball and cone joints. The ETS is an alpha-class tool designed to demonstrate full-field EUV imaging and provide data to equipment manufacturers to support production-tool development.

Experimental modal tests were conducted on the supported POB, prior to applying the damping treatment, to determine the corresponding modes of vibration. The tests focused on the rigid body motions of the POB on the bipod flexures, as opposed to the flexural modes of the POB itself. These modes were either rocking or lateral motions of the POB, either front to back or side to side.

Ideally the experimental modal testing of the POB would be performed in the end use configuration; that is, with the POB supported on the bipod flexures and kinematically mounted to the ETS. However, this was not possible because the testing occurred prior to the construction of the ETS. Therefore, a mass-equivalent steel plate was used to represent the ETS for testing purposes. The plate was approximately 52 inches square, 3 inches thick, and weighed approximately 2100 lbs (9341 *N*). This provided a high stiffness comparable to what would be expected on the isolation frame of the ETS where the POB would mount. An opening was cut in the center of the plate that would allow the POB to be supported by the three bipod flexures. Three stainless steel balls, ¾ of an inch in diameter, were epoxied into countersunk holes on the top surface of the plate at the locations where the POB support flexures would interface with the ETS.

To best approximate free boundary conditions for the modal tests, and thus avoid altering the dynamics of the system, the plate was suspended from an overhead crane using elastic bungee cords. Frequency response functions (FRF) of the system were obtained by exciting the plate and measuring the response output at 54 different locations on the POB structure, flexures, and plate with a sensitive tri-axial accelerometer (1V/G). Initially the plate was excited using a large force hammer as shown in *Figure 5* below; however, it was later changed to a small electromagnetic shaker with the stinger positioned normal to the plate surface. The shaker provided well-controlled excitation levels, more comparable to what might be expected on the actual system. The shaker was setup to transmit a random broadband force with a bandwidth of 500 Hz to the plate. The input force from the shaker to the plate was measured with a load cell (100 mV/lbf). *Figure 6* shows a sample frequency response measurement obtained from testing a particular point on the POB.

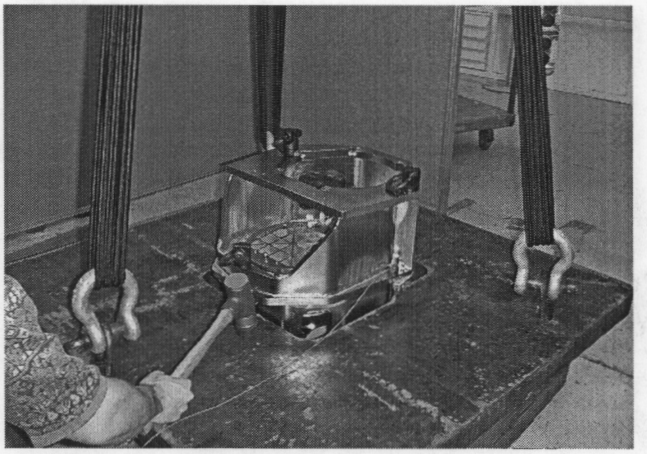

Figure 2: Experimental modal testing of the POB mounted to an ETS mass-equivalent steel plate.

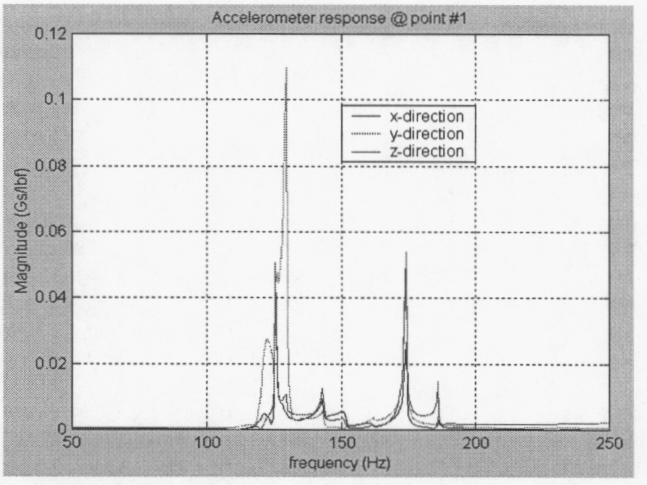

Figure 6: FRF of sample point on POB structure.

Once frequency response functions (FRF's) were obtained, they were analyzed and curve-fitted using a commercially available modal analysis software package. Curve fitting helped to identify frequency and damping parameters as well as mode shape information extracted from model animations. The animations of the individual mode shapes helped distinguish plate modes from rigid body rocking modes of the POB on its support flexures. The plate modes are not of interest since they will not be in the real system. A total of three plate modes were identified; one torsional mode and two bending modes. Ideally these plate modes would occur at frequencies either much higher or lower than the POB modes, thus minimizing the effort in analyzing the modes of interest. Unfortunately, they occurred in the same range of frequencies as the POB modes, which complicated the analysis. *Table 1* below shows the extracted modal parameters of frequency and damping for the system up to 300 Hz. The table also indicates whether the modes are plate modes or modes associated with the POB on the support flexures. *Figure 7* shows an overlay magnitude plot of all the measured frequency response functions with pointers denoting which modes are plate modes and which are POB modes.

Table 1: Extracted modal parameters from the experimental data (no damping treatment added)

Mode	Freq. (Hz)	Damping (% critical)	Damping factor (Hz)	Type of mode
1	121.3	1.15	1.395	POB mode
2	125.6	0.12	0.151	plate mode
3	129.3	0.32	0.414	POB mode
4	143.1	0.34	0.487	POB mode
5	151.1	0.94	1.420	POB mode
6	161.4	1.01	1.630	POB mode
7	173.8	0.20	0.357	plate mode
8	186.1	0.13	0.242	plate mode

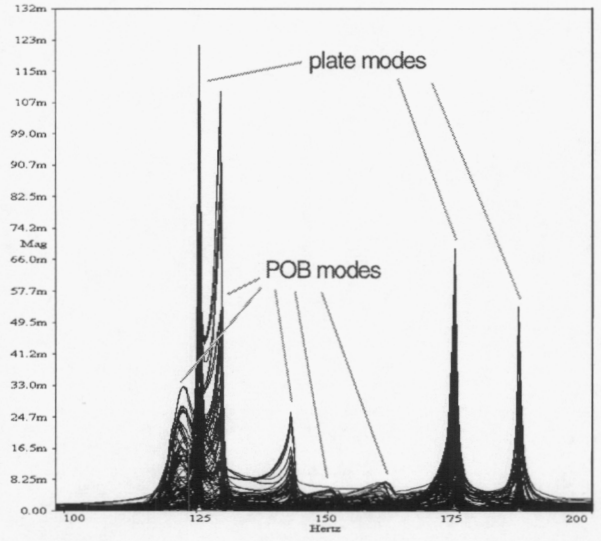

Figure 7: Overlay magnitude plot of measured FRF's without damping treatment added.

There is very little damping associated with the rigid body motions of the POB, as is evidenced by the extracted damping values in *Table1*. All modes have approximately 1% or less of critical damping. This is quite undesirable and effectively means that vibration occurring in the isolation frame of the ETS near the resonant modal peaks, will be transmitted to the POB and amplified by a factor of 50 or more. The constrained-layer damping treatment will significantly reduce this amplification.

FINITE ELEMENT MODELING OF TEST SETUP

As part of the dynamic study for the supported POB, a detailed finite element model was created and analyzed. This model is shown in *Figure 8* below.

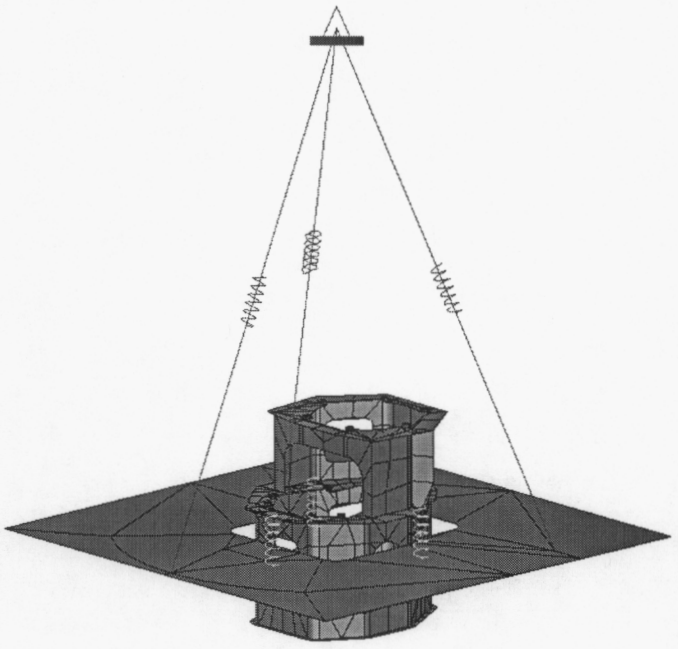

Figure 8: Finite element model of POB structure mounted to ETS mass equivalent plate using bipod flexures.

Modeling the system was fairly straight forward with exception to the ball and cone joints, which were modeled using spring elements. The radial and axial stiffness of these joints were calculated using Hertzian-contact theory. These values were then fine tuned so that the analytical modal results matched closely with the experimental results both in frequency and mode shape. Comparison of the analytical and experimental results showed very good agreement for all modes, except for the 5th POB mode (161.4 Hz) which was not predicted by finite element modeling (see *Table 2*). The model animations from the experimental data suggest that the motion of this mode could be dependent on the friction in the ball and cone joint interface, which was not modeled. Fortunately this mode is not expected to impact the motion of the projection optics compared to the first three POB modes. The first three POB modes are primarily excited by vertical disturbances, while the fourth and fifth modes are primarily

excited in the lateral direction. On the ETS, virtually all excitation will come as a result of ground input disturbances with the vertical component at least one to two orders of magnitude larger than the lateral components.

Table 2: Comparison between analytical results using a finite element model and experimental results.

Mode	FEA Prediction	Experimental Measurement	Type of Mode	% Difference
1	122.2 Hz	121.3 Hz	POB mode	0.74
2	123.8 Hz	125.6 Hz	plate mode	1.43
3	131.9 Hz	129.3 Hz	POB mode	2.01
4	143.5 Hz	143.1 Hz	POB mode	0.28
5	136.8 Hz	151.1 Hz	POB mode	9.46
6	not predicted	161.4 Hz	POB mode	-
7	168.6 Hz	174.8 Hz	plate mode	3.54
8	184.5 Hz	186.1 Hz	plate mode	0.86

FINITE ELEMENT MODELING OF BIPOD FLEXURES TO DETERMINE OPTIMUM VISCO-ELASTIC STIFFNESS

In order to determine the optimum visco-elastic stiffness and design the optimal damping in the support flexures, a finite element model of one of the support legs was created. This model incorporated a thin visco-elasitic layer and a constraining layer on both sides of the bipod flexure leg. The leg was constrained at one end and axially loaded on the other end. The visco-elastic material was modeled having a thickness of 0.010 *in.* (0.254 mm) and a surface area of 1.24 $in.^2$ (800 mm^2) per side. The webs and constraining-layers were modeled with a thickness of 0.040 *in.* (1.016 mm). *Figure 9* shows the model of the support flexure leg used in the finite element analyses.

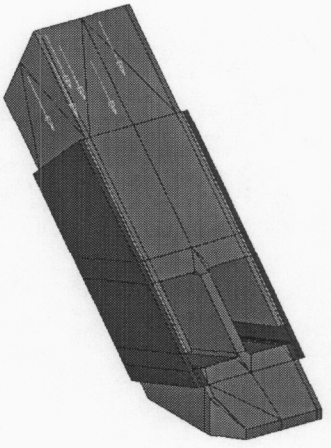

Figure 9: Finite element model of support flexure leg.

A finite element method was chosen because of the difficulties associated with determining the correct value of α_{opt} using conventional analytical methods. When using finite element methods, the design goal is to find the relevant properties of the visco-elastic layer, such as shear modulus, area, and thickness, that maximize the proportion of strain energy in the VEM. This is analogous to finding α_{opt} as described in equation (6) for the simple spring model.

The optimal visco-elastic stiffness, k_v, was determined by performing a series of analyses on the model in which the visco-elastic stiffness was varied over some range. After each analysis the strain energy in the visco-elastic elements was summed and the total strain energy of the model was calculated. The ratio of these two strain energy values was then compared for each analysis. It was easy to vary the visco-elastic stiffness by varying the modulus of elasticity of the visco-elastic elements. The relationship between modulus of elasticity and visco-elastic stiffness is shown in the following equations:

$$k_v = \frac{G \cdot A}{t} \quad \text{and} \quad G = \frac{E}{2 \cdot (1+\nu)} \quad \therefore \quad k_v = \frac{E \cdot A}{2t \cdot (1+\nu)} \qquad (8)$$

where G is the shear modulus of the material, A is the surface area covered by the material, t is the thickness of the material, and ν is Poisson's ratio. By varying the modulus of elasticity (E) no modifications to the model's dimensions were necessary. Once all the analyses had been performed the strain energy ratio of $u_{visco\text{-}elastic} / u_{total}$ was plotted against visco-elastic stiffness, as calculated by eqution (8). *Figure 10* shows this plot, from which the optimal visco-elastic stiffness, $k_v|_{opt} \approx$ 830,000 lbf/*in* (145,355 N/mm) can be identified. The shape of the plot is similar to the imaginary part of the equivalent stiffness shown in *Figure 4*, as expected. At this stiffness approximately 13% of the strain energy associated with the axial load is absorbed by the visco-elastic elements. This may seem small, but as shown later will have a significant affect on reducing vibrational amplitudes at resonance.

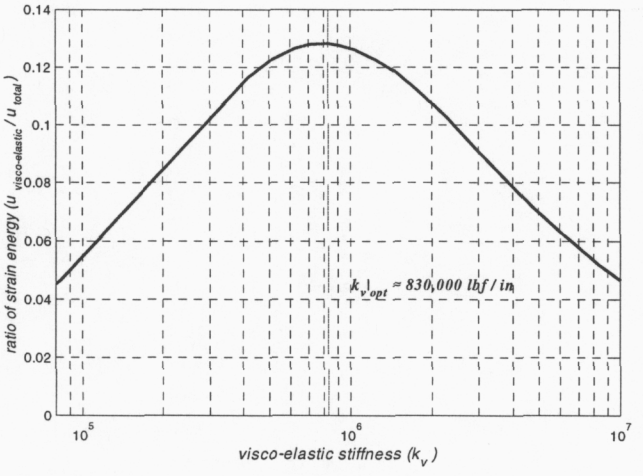

Figure 10: Plot of strain energy ratio vs. visco-elastic stiffnes computed from finite element analyses.

Once the optimal visco-elastic stiffness had been identified using the finite element method, it was used to determine the actual parameters to be used on the POB support

flexures. Because the ETS has strict out-gassing requirements, there was only one choice of visco-elastic material available for use. The material came in sheet form with a specified thickness of 0.001, 0.002, or 0.004 inches. The shear modulus and loss factor of the material are both temperature and frequency dependent and the values for each were obtained using a specified nomograph provided by the manufacturer of the visco-elastic material.

It was desirable to dampen at least the first two modes of vibration of the POB, which occur at frequencies of 121.3 Hz and 129.3 Hz. The shear modulus of the selected visco-elastic material at an operating temperature of 20 ºC for these frequency values was approximately 1,160 *psi* (8 *Mpa*). For convenience in applying the visco-elastic material to the flexure webs, a material thickness of 0.004 inches (0.1016 mm) was chosen. With two of the three variables that make up the visco-elastic stiffness already determined, the last was easily solved for in the following manner:

$$k_v = \frac{G \cdot A}{t} \Rightarrow k_v\big|_{opt} \approx 830{,}000 \text{lbf/in} = \frac{(1160\,\text{psi}) \cdot A}{0.004\,\text{in.}} \therefore A \approx 2.9\,\text{in}^2 \quad (9)$$

It was determined that a total surface area of approximately 2.9 *in²* (1,840 *mm²*), or approximately 1.45 *in²* (920 *mm²*) for each side, was required to optimally damp out frequencies in the range of 120-130 Hz. The constraining-layers and visco-elastic material were designed and fabricated to accommodate this desired surface area.

MODAL TESTING OF BIPOD SUPPORT FLEXURES WITH DAMPING TREATMENT ADDED

In order to determine the effectiveness of the optimized constrained-layer dampers, a series of experimental modal tests were performed on the POB system. The exact same testing procedure was followed as originally used to determine the modal parameters listed in *Table 1* so that valid comparisons could be made before and after the dampers were added. Upon collecting all the frequency response data, it was plotted and analyzed with the modal software package as previously described. *Figure 11* shows an overlay of magnitude plots for all the frequency response functions collected.

It is obvious from the plotted data in *Figure 11* that the dampers have virtually eliminated the POB modal peaks. The three prominent modes shown in *Figure 11* were identified as being the same plate modes as reported in *Table 1*. The second and third plate modes have had a measurable increase in damping that results because these modes are bending modes that cause a piston motion of the POB structure. This piston motion exercises the dampers and reduces the vibration amplitude. The first plate mode is torsional and does not couple well to the POB structure through the three-point mount. Therefore the torsional mode does not exercise the dampers and consequently there is no increase in damping. A comparison of measured damping values for the plate modes is shown in *Table 3*.

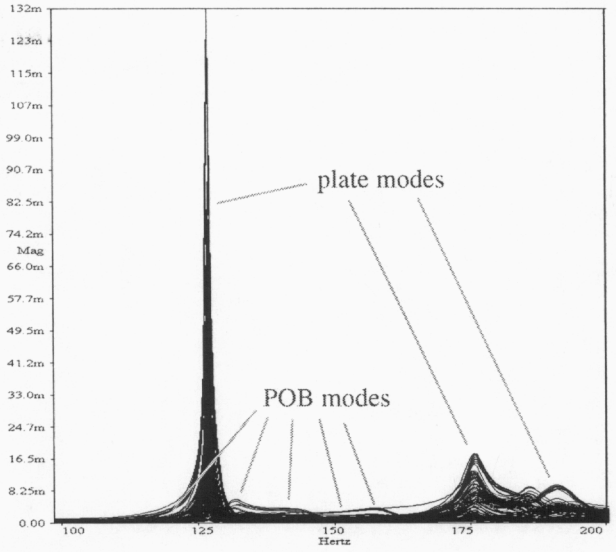

Figure 11: Overlay magnitude plot of measured FRF's with damping treatment added.

Table 3: Comparison of extracted damping parameters for the plate modes, with and without dampers added.

	Without Dampers		With Dampers	
Plate mode	Freq. (Hz)	Damping (ζ) (% critical)	Freq. (Hz)	Damping (ζ) (% critical)
1	125.6	0.12	126.9	0.13
2	173.8	0.20	175.6	1.10
3	186.1	0.13	190.1	1.00

Extracting modal parameters from the POB modes was more difficult since all of the modal peaks had virtually disappeared from the data. The problem in identifying modal parameters for the first two POB modes was that the torsional plate mode was so dominant by comparison that the damped POB modal peaks were hidden in most of the collected FRF's. The other three modes, although less influenced by the plate modes, had dropped in magnitude to such a degree that the noise floor of the sensor influenced much of the data. The only FRF's used in the parameter estimation were those where the response of the plate modes was minimum and the response of the POB modes were fairly significant. A comparison of the extracted modal parameters, with and without constrained-layer damping added, is shown in *Table 4* below. Included in the table is the quality factor (Q.F), which is a measure of vibration amplitude at resonance.

Table 4: Comparison of extracted damping parameters for the POB modes, with and without dampers added.

	Without Dampers			With Dampers		
POB mode	Freq. (Hz)	Damp. (ζ)	Q.F. (Q)	Freq. (Hz)	Damp. (ζ)	Q.F. (Q)
1	121.3	1.15	33.3	122.5	8.40	5.90
2	129.3	0.32	156.3	131.5	7.00	7.10
3	143.1	0.34	147.1	145.3	2.71	18.5
4	151.1	0.94	53.2	152.0	2.45	20.4
5	161.4	1.01	49.5	159.8	2.40	20.8

CONCLUSIONS

The projection optics system for extreme ultraviolet lithography (EUVL) requires precise and repeatable alignment of the reflective optics within the structural housing, referred to as the projection optics box (POB). It is critical that the POB is isolated from variable quasi-static loads that could change the optical alignment. Such loads could arise from being mounted in an over-constrained manner. To minimize influence to its natural shape, the POB is exactly constrained using a unique kinematic coupling. It consists of three ball-cone joints to provide a repeatable connect-disconnect interface between the POB and the mounting frame (i.e. the engineering test stand (ETS)). Each joint allows three rotational degrees of freedom about the ball center, while a pair of blade flexures at the other end (one in each leg) provides an additional hinge axis that in combination with the ball-cone joint releases one translational constraint. Therefore, each joint constrains exactly two degrees of freedom and three such joints, properly placed, exactly constrain the six rigid-body degrees of freedom of the POB.

Dynamic motion of the POB is also a concern because it causes the image to move with respect to the wafer. Experimental modal tests were performed to determine the resonant modal frequencies of a nearly rigid POB moving on its supports. The measured damping was quite low, which means that vibration occurring on the mounting frame near resonant modal peaks will be transmitted to the POB and significantly amplified. As a means of reducing amplification at resonance, constrained-layer dampers were added to the support flexures. These dampers were designed to reduce the resonant peaks of the first three POB modes, with emphasis on the second mode. Experimental tests confirmed the effectiveness of the dampers. The quality factor (Q), which measures the amplification at resonance, dropped from 33.3 to 5.9 for the first mode, from 156.3 to 7.1 for the second mode, and from 147.1 to 18.5 for the third mode. These dampers will help ensure that the assembled POB meets the stringent vibration requirements necessary to produce high quality optical images.

REFERENCES

Hale, L.C., "*Principles and Techniques for Designing Precision Machines*", PH.D. Thesis, M.I.T., Cambridge Massachusetts, Feb. 1999

Marsh, E.R., "*An Integrated Approach to Structural Damping*", Ph.D. Thesis, M.I.T., Cambridge Massachussets, 1994

Marsh, E.R., Hale, L.C., "*Damping of Flexural Waves with Imbedded Viscoelastic Materials*", ASME Journal of Vibration and Acoustics, Vol. 120 No.1, pp. 188-193, 1998

Wilke, P.S., Decker, T.A., Hale, L.C., "*Highly-Damped Exactly-Constrained Mounting of an x-ray Telescope*", SPIE, Passive Damping, Vol. 2445, March 1995

Marsh, E.R., Hale, L.C., "*Damping Machine Tools with Imbedded Viscoelastic Materials Constrained by a Shear Tube*", Proc. ASME Design Engineering Tech. Conf., ASME DE, Vol. 84-3, pp. 9-14, Boston, MA, 1995

Johnson, C., Kienholz, D., "*Finite Element Prediction of Damping in Structures with Constrained Viscoelastic Layers*", American Institute of Aeronautics and Astronautics, Vol. 20, pp. 1284-1290, 1982

Slocum, A.H., "*Precision Machine Design*", Prentice Hall, Englewood Cliffs, New Jersey, 1992

Thomson, W.T., Dahleh, M.D., "*Theory of Vibration with Applications*", Prentice Hall, Upper Saddle River, New Jersey, 1998

*This work was performed under the auspices of the U.S. Department of Energy by University of California Lawrence Livermore National Laboratory under contract No. W-7405-Eng-48.